

SCANNING PROBE MICROSCOPY ACROSS DIMENSIONS

Ille C. Gebeshuber^{1,2}, Richard A. P. Smith², Hannspeter Winter² and Friedrich Aumayr²

¹ Austrian Center of Competence for Tribology AC²T research GmbH, Viktor Kaplan-Straße 2, 2700 Wiener Neustadt, Austria

² Institut für Allgemeine Physik, Technische Universität Wien, Wiedner Hauptstraße 8-10/E134, 1040 Vienna, Austria

Abstract. Scanning probe microscopy offers interesting approaches to not only image but also manipulate samples in the micro- and nanoscale regime. Atomic force microscopy became one of the most versatile microscopy methods in biology, since this type of microscopy works under ambient conditions and in many cases, no extensive sample preparation is necessary. From imaging single living cells to large protein molecules and even more interestingly protein-protein interactions in real time, to micro- and nanoscale investigations of mechanical parameters such as viscoelasticity, atomic force microscopy has proved a useful technique. Imaging biomolecules at atomic resolution is a dream which might come true within the next few years. A powerful new technique is magnetic resonance force microscopy, combining three-dimensional magnetic resonance imaging with the excellent force sensitivity of the atomic force microscope. This type of microscopy opens the possibility of performing scanning probe magnetic resonance imaging with a sensitivity more than 10 million times better than the sensitivity of the medical magnetic resonance imaging devices for visualizing of organs in the human body. This improved sensitivity extends magnetic resonance imaging into the nanometer realm.

Keywords: AFM, Diatoms, Frustule

1. SCANNING PROBE MICROSCOPY

In the early 1980ies of the last century, researchers at the IBM Zürich research laboratories invented a new type of microscope: the scanning tunneling microscope (STM, [1]). This instrument, which proved capable of imaging solid surfaces with atomic resolution, revolutionized microscopy and surface analysis in an unprecedented way.

The inventors of the STM, Gerd Binnig and Heinrich Rohrer, were awarded the Nobel Prize in Physics in 1986 (together with Ernst Ruska, who was honored for the design of the first conventional electron microscope).

The STM stimulated the development of a whole family of scanning probe methods (SPM) that are all based on instrumental principles very similar to that of the STM:

- atomic force microscopy (AFM)
- scanning near field optical microscope (SNOM)
- magnetic force microscope (MFM)
- magnetic resonance force microscope (MRFM)
- scanning thermal microscope
- scanning potentiometry microscope
- ballistic electron emission microscope (BEEM)
- scanning capacitance microscope
- scanning ion conductance microscope (SICM)

The most popular offspring are the atomic force microscope (AFM) [2], and the scanning near-field optical microscope (SNOM) [3]. For an introduction to AFM for biologists see [4].

A scanning probe microscope basically works like an old fashioned record player, where the up-down movement of the needle sends the recorded impulse through the amplifier and on to the speakers to produce music. For a generalized scheme of an SPM, see Figure 1.

A very sharp "needle", called the probe, scans over the surface of a material. The movement of the needle, due to the interactions between the needle and the atoms in the surface, are detected by a computer and sent to produce an image of the surface on a computer screen. A close examination of any minute changes occurring to the atoms hereby becomes relatively simple.

The mechanical, electrical, magnetic, optical and chemical interactions between the sharp probe and the surface provide a 3D representation of surface parameters at or near the atomic scale. The samples can be in air, vacuum or immersed in some liquid.

The areas and opportunities for SPM based investigation are vast indeed: they cover semiconductor chips, polymers, chemicals, coatings, paper, metals, ceramics, magnetic and recording materials, medicine, biological substances, cells, tissues, films and so on and on through the natural and applied sciences.

STM, AFM and SNOM today represent a set of microscopy techniques that can be applied in many different and highly dedicated modes of operation, such that a variety of physical and chemical properties of a material becomes accessible. This versatility of SPM in general is, apart from the inherent high resolution, its major strength.

Today no scientist can master more than a few of all the microscopy methods based on static electric and magnetic fields, particle beams, electromagnetic radiation, acoustic waves, etc., and presumably would not have access to the instrumentation necessary to apply a number of them. On the other hand the operational principle of SPM is uniform, and often a variety of physical properties can be obtained even by employing only one general-purpose set-up [5].

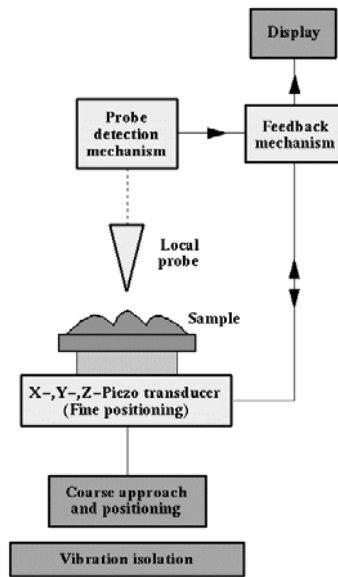


Figure 1. Generalized scheme of a scanning probe microscope (SPM). Image taken from <http://spm.phy.bris.ac.uk/techniques/images/SPMschematic.gif>.

1.1. Scanning Tunneling Microscopy

The operation of a scanning tunneling microscope is based on the so-called tunneling current, which starts to flow when a sharp tip approaches a conducting surface at a distance of approximately one nanometer. The tip is mounted on a piezoelectric tube, which allows tiny movements by applying a potential difference between sample and tip. Thereby the electronics of the STM system control the tip position in such a way that the tunneling current and, hence, the tip-surface distance is kept constant, while at the same time scanning a small area of the sample surface. This movement is recorded and can be displayed as an image of the surface topography. Under ideal circumstances, the individual atoms of a surface can be resolved and displayed.

It should be noted, however, that STM images not only display the geometrical structure of the surface, but also depend on the electronic density of states of the sample, as well as on special tip-sample interaction mechanisms that are not yet fully understood.

Although the STM itself does not need a vacuum (it works in air as well as under liquids), ultra high vacuum (UHV) is required if one needs to avoid contamination of the samples by the surrounding medium.

A problem in the investigation of metal surfaces is the fact that these surfaces appear very flat to an STM, i.e., the apparent height of individual atoms (corrugation) is 1/100 to 1/10 of an atomic diameter. Therefore, for resolving individual atoms the distance between the tip and the sample must be kept constant within 1/100 of an atomic diameter or less (approx. 0.002 nm). This demands not only very high rigidity of the STM itself but the STM must also be efficiently decoupled from environmental vibrations.

For introductory texts on STM see [6-8].

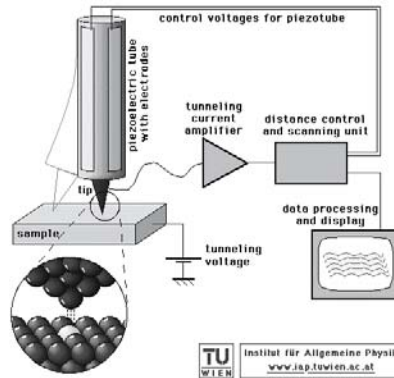


Figure 2. Generalized scheme of a scanning tunneling microscope (STM). Image taken from http://www.iap.tuwien.ac.at/www/surface/STM_Gallery/stm_schematic.html.

1.2. Atomic Force Microscopy

The atomic force microscope measures the interaction force between the tip and the surface. A very sharp tip (cantilever) is scanned across the sample surface using piezoelectric scanners (Fig. 3). The tip may be dragged across the surface or may vibrate as it moves.

The measurement is monitored using the so-called optical beam reflection detection system, in which a laser beam is reflected from the reverse side of the cantilever onto a four quadrant position-sensitive photo sensor. This detector measures the bending of cantilever while the tip is scanning over the sample. The measured cantilever deflections are used to generate a map of the surface topography.

AFM can be used to study insulators and semiconductors as well as electrical conductors, biological samples, magnetic samples, etc.

Three imaging modes, contact, non-contact and intermittent contact (tapping) mode, can be used to produce topographic images of sample surfaces.

In **contact mode**, the tip makes physical contact with the sample and is essentially dragged across the sample surface to make a topographic image. Contact mode imaging can be performed within a liquid environment, which essentially eliminates problems caused by surface moisture such that much lower contact forces can be used.

In **non-contact mode** the cantilever is vibrated near the surface of a sample. The spacing between the tip and the sample is of the order of tens to hundreds of angstroms. Like contact mode, the motion of the scanner is used to generate the topographic image.

Intermittent mode (tapping mode) is like contact mode except for that the vibrating cantilever tip is brought closer to the sample so that it just barely hits (i.e. taps) the sample [9]. This mode is applicable to both imaging in liquids and in air, particularly for soft samples, as the resolution is similar to contact mode while the lateral forces applied to the sample are lower and less damaging.

In **phase imaging** the phase difference between the oscillations of the cantilever driving piezo and the detected oscillations yields information concerning stiffness and viscoelasticity of the sample.

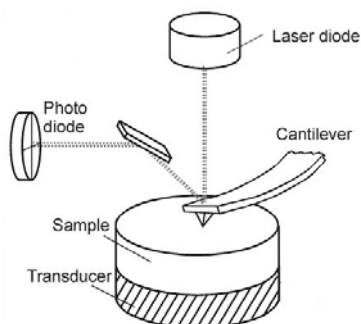


Figure 3. Generalized scheme of an atomic force microscope (AFM). Image by P.K. Hansma (UCSB), taken from <http://www.soest.hawaii.edu/~zinin/Zi-AFM.html>.

1.3. Scanning Near Field Optical Microscopy

SNOM (Scanning Near Field Optical Microscopy) is a technique that enables work with standard optical tools beyond the diffraction limit which normally restricts the resolution capability of conventional microscopy [3].

It works by exciting the sample with light passing through a sub-micron aperture formed at the end of an optical fibre. Typically, the aperture is a few tens of nanometers in diameter. The fibre is coated with metal to form an aperture and to prevent loss of light, thus ensuring a focused beam from the tip.

SNOM is capable of imaging a variety of fine structures, showing great application potential in life science, material science and semiconductor technology. With spectroscopy, SNOM can realize local spectra, fluorescence sensing and single atom/molecule detection and identification.

1.4. Scanning Ion Conductance Microscopy

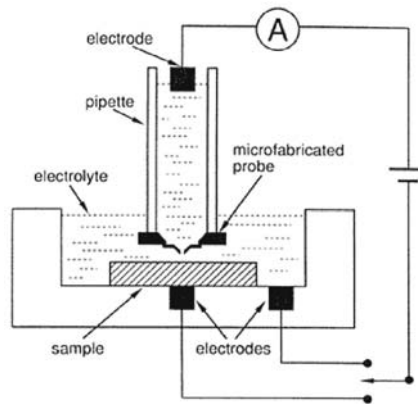


Figure 5. Generalized scheme of a scanning ion conductance microscope (SICM). Reprinted with permission from [10].

The scanning ion-conductance microscope (SICM) can image the topography of nonconducting surfaces that are covered with electrolytes ([11], Figure 5). The probe of the SICM is an electrolyte-filled micropipette. The smaller the opening diameter of the pipette, the better the resolution of the microscope (resolution equals about half the diameter of the pipette).

The SICM measures the ion current between two electrodes, one in the glass micropipette, the other one in the bath solution. The flow of ions through the opening of the pipette is blocked at short distances between the probe and the surface, so limiting the ion conductance.

A feedback mechanism can be used to maintain a given current and in turn determine the distance to the surface. The SICM can also sample and image the local ion currents above the surface.

SICMs are currently not commercially available. We constructed our own SICM [12]. Human red blood cells (sample donated by Stefan Schraml) in Nomarski mode and imaged with our home-built SICM are shown in Figure 6.

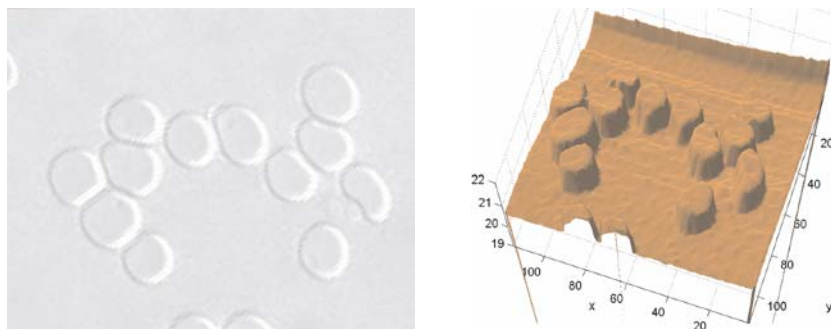


Figure 6. Nomarski light microscopy (left) and Scanning Ion Conductance Microscopy images of human red blood cells in buffer solution on a glass slide [12]. $100\mu\text{m} \times 100\mu\text{m}$ scan size.

2. CELLS

Since many scanning probe microscopes also work in liquids, it is possible to obtain high resolution images of living cells with this type of microscopy.

Below, a couple of interesting examples of SPM investigations on living cells from our own research as well as from other groups are given.

2.1. Diatoms

Diatoms are unicellular organisms with a size of some micrometers. Their surfaces consist of a siliceous skeleton (amorphous glass) enveloped by an organic case.

Individual diatoms range from 2 micrometers up to several millimeters in size, although only few species are larger than 200 micrometers. Diatoms as a group are very diverse, with 12 000 to 60 000 species reported [13]; most of them of exquisite beauty (see Figs. 7 and 8). These naturally nanostructured organisms reproduce via cell division: under ideal conditions,

within ten days the offspring of one single cell would number one billion cells (natural “assembly line production” of nanostructures)!

Diatoms live in various wet environments, such as saltwater or freshwater and on wet surfaces. They can either be freely floating (planctonic forms) or be attached to substrates like rocks or plants (benthic forms).

These unicellular organisms are interesting from the point of materials science and biomimetic studies, since they master challenges as diverse as building nanostructured glass shells with high load capacity (a problem interesting for lightweight structures architecture) and engineering strong and robust adhesives that are stable in wet environments (most man-made adhesives fail to bond in wet conditions, owing to chemical modification of the adhesive or its substrate). Furthermore, diatoms excel at preventing dissolution of their silica shells in water owing to a covering layer (up to date technology is currently facing the problem that man made glass fiber reinforced polymers show rapid deterioration when used in water).

Diatoms are small, mostly easy to cultivate, highly reproductive and, since many of them are transparent, they are accessible by different kinds of optical microscopy methods. For an overview of diatoms see [14].

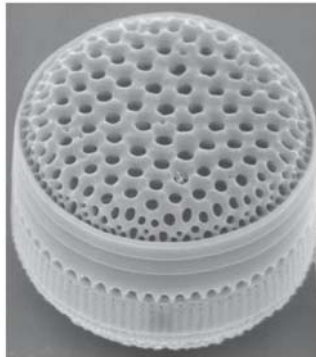


Figure 7. Scanning electron microscope image of a diatom. © W. Oschmann.

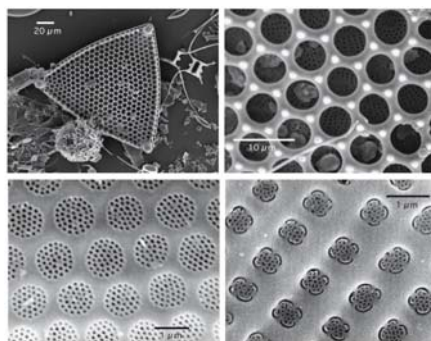


Figure 8. Naturally nanostructured surfaces. The top left image shows an SEM image of a whole cell of *Tricaeratium favus*, the top left image is a zoom into the left image. The bottom images are surfaces of two other species, *Roperia tessellata* and *Achnathes brevipes*. Reprinted with permission from [15].

Currently, human chemical synthesis cannot produce siliceous structures with the hierarchical structural detail of the diatom skeletons nor can ordered siliceous structures be produced synthetically under the benign conditions of diatom biomineralisation [15].

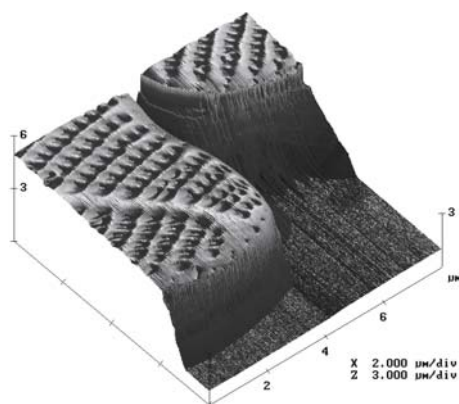


Figure 9. AFM image of parts of two living diatom cells of the species *Navicula seminulum* growing on a glass slide. Note that the flat area does not correspond to the surface of the glass slide, but is determined by the maximum possible extension of the z-piezo of the microscope. Image acquired using AFM contact-mode imaging in water, imaging parameter topography, scan size $8 \times 8 \mu\text{m}^2$, scanning frequency 1 Hz. Reprinted with permission from [16].

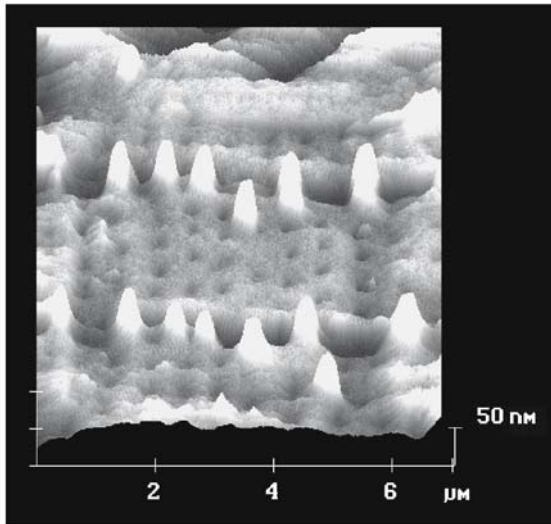


Figure 10. Using the AFM cantilever as a tool. A $5 \times 5 \mu\text{m}^2$ area is repeatedly scanned in AFM contact mode at high feedback force (about 100 nN). After 2 days, a slightly larger area comprising the area where the organic layer had been worn away meanwhile is imaged, revealing a height of the organic layer of about 10 nm. Contact mode, topography, scan size $7 \times 7 \mu\text{m}^2$, scanning frequency 2 Hz. Reprinted with permission from [16].

Atomic force microscopy offers the opportunity to image these interesting cells alive in ambient conditions, under water, as they continue to grow [16], (see Figure 9).

Since in atomic force microscopy tip is (in contact mode) dragged with 'physical contact' over the sample, the AFM cantilever can also be used as a tool to mechanically modify the sample. For example, it is possible to determine the thickness of the organic coating enveloping the siliceous skeleton in diatoms by repeatedly scanning (with increased force) a selected area, and imaging a slightly larger area some time later: the altered area is about 10 nm 'lower' than the unaltered surface (see Figure 10).

2.2. Biogenic Adhesives

Most state-of-the-art man-made adhesives fail to bond in wet conditions, owing to chemical modification of the adhesive or its substrate. Engineering strong and robust underwater adhesives that are stable in wet environments is a challenge to current technology. Knowledge of the intrinsic properties of natural adhesives might give valuable information for future engineering approaches.

Three different species of benthic freshwater diatoms (*Eunotia sudetica*, *Sellphora seminulum* and a yet unidentified species) were selected for their

strong adhesives by exposure of a greater number of species to highly selective environmental conditions [16].

Eunotia sudetica is very convenient for *in situ* AFM investigation of the diatom adhesive at the cell interface because there is barely any cleft between adjacent cells (Fig. 11a), and valve undulations are less pronounced than in the other species investigated. The diatom adhesive is apparent as small topographic features at the cell interface. The bead-like structures are 10–20 nm high, have lateral dimensions of about 1 μm and are about 1 μm apart. The phase image (Fig. 11b) clearly depicts the altered viscoelastic properties of these structures: the diatom adhesive causes a phase shift of up to 10° compared with the phase difference on the rest of each of the two frustules, where it is within 1° on each, apart from a 2° phase jump between the two adjacent valves. Such a phase jump between cells also appears in the other species where the adhesives are not accessible because of deep clefts between the single organisms.

To access the adhesive *Eunotia sudetica* produces for its attachment to the glass slide on which the cells grow, a *Eunotia sudetica* cell was mechanically removed using a scanning tunneling microscope tip on a micromanipulator stage [15]. Then, the AFM cantilever is brought into contact with the adhesive and lifted upwards again. The force applied after the tip makes contact with the surface can provide a measurement of the stiffness or compliance of the sample while the force required to pull the sample up from the surface is a measure of the adhesion between the tip and the sample. Figure 12 shows such force–distance curves for the diatom surface and the natural adhesive that attaches *Eunotia sudetica* to the glass slide. The diatom surface is less elastic and “sticky” than the adhesive. Several bond-breaking events occur when trying to retract the cantilever from the biogenic adhesive and the pulling force must be applied over nearly one micrometer to completely remove the cantilever. The multiple unbinding events, although not in the monomolecular regime, are similar to the curves found to provide the molecular mechanistic origin of the toughness of natural adhesives, fibres and composites [17].

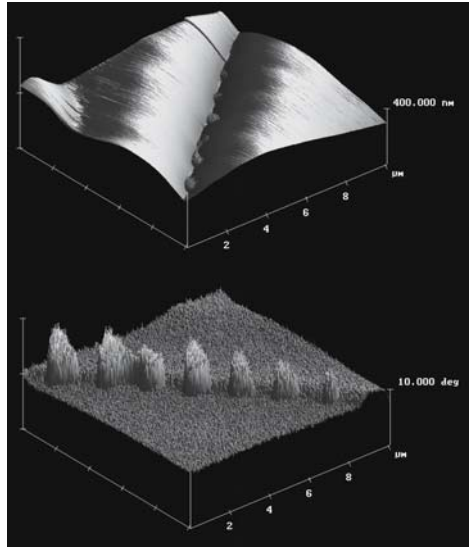


Figure 11: (a) The adhesives in the contact region of two cells of *Eunotia sudetica* are apparent as small topographic features on the slightly undulating cell interface. The corrugation of the bead-like structures is between 10 and 20 nm and their lateral dimension and spacing is about 1 μm . (b) In the phase image these features are far more striking. The diatom adhesive causes a phase lag of about 10° compared with the rest of the frustule surfaces, where on a single frustule it is within 1° . Note the 2° interfrustule phase step, which reveals slightly different viscoelastic properties of the two neighboring valves. Tapping mode, topography and phase, scan size $10 \times 10 \mu\text{m}^2$, scan rate 5 Hz. Note that for better view (b) is rotated clockwise by 90° as compared with (a). Reprinted with permission from [16].

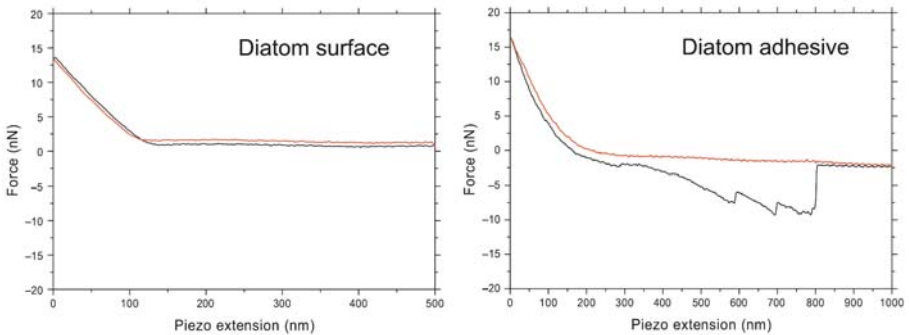


Figure 12: Force–distance curves. Left: No adhesion can be recognized on the diatom surface. Right: Representative data for the diatom adhesive that attaches *Eunotia sudetica* to the substrate. Note that several debonding events occur and that the pulling force must be applied over nearly one micrometer to completely debond the cantilever from the surface. Reprinted with permission from [16].

2.3. Biotribology

Tribology is the study of friction, adhesion, lubrication and wear. Technical micro- and nanosystems often experience failure (e.g. stiction = static friction) due to the lack of reliable concepts, whereas biological systems are reliable also at this scale.

There is an increasing need for a multidisciplinary, system-oriented approach to manufacturing micro- and nanoelectromechanical systems (MEMS/NEMS) that function reliably. Comprehensive understanding of tribology at the micro- and nanoscale can only be achieved through the cross-fertilization of ideas from different disciplines and the systematic flow of information and people among research groups.

Biomicro- and -nanotribology is a new interdisciplinary field of research combining methods and knowledge of physics, chemistry, mechanics and biology. The aim of biotribology is to gather information about friction, adhesion, lubrication and wear of biological systems and to apply this knowledge to innovate technology, with the additional benefit of environmental soundness.

Biological systems with moving parts have optimised their lubrication during evolution. Some diatom species can serve as interesting model organisms for nanotribological investigations:

Bacillaria paxillifer is a motile colonial diatom (Fig. 13). Entire colonies of 5 to 30 cells expand and contract rhythmically and in a coordinated manner. In motion, the cells glide along each other. No wear has ever been detected in this species. Effective biogenic lubricants might have evolved to protect the single cells.

Ellerbeckia arenaria is a colonial diatom which lives in waterfalls. The string-like colonies can be several millimeters long and can be elongated by about one third of their original length. When released, they return to the original position like a spring [18]. This interesting feature could suggest that there are parts in relative motion in this species, coping with friction and wear.

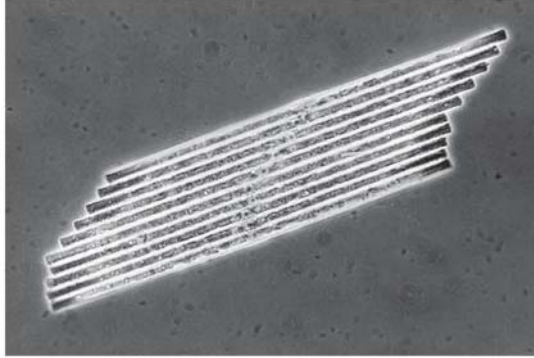


Figure 13: Bacillaria paxillifer colony with 10 cells. In motion, colonies expand and contract rhythmically and in a coordinated manner, with the cells gliding along each other. Biogenic lubricants might have evolved to protect the single cells from wear. © Wim van Egmond, Microscopy-UK (<http://www.microscopy-uk.org.uk/>).

Eunotia sudetica is a colonial diatom. AFM investigations of living cells reveals bead-like features which might well act as friction reducers, either by means of ball-bearings or a solid lubricant or a strategy which still is completely unknown to engineers.

For an introduction to diatom bionanotribology, see [18 ,19].

3. SINGLE MOLECULES

The AFM has proven to be a useful tool for studying proteins at the single molecule level. In particular, the AFM has been used to measure both structural and mechanical properties of individual proteins in physiologically relevant buffer solutions.

3.1. Chaperonins: Probing Protein-Protein Interactions in Real Time

The *E. coli* chaperonin GroEL and its cochaperonin GroES play important roles in helping proteins to reach their native states. GroEL and GroES work together in a series of adenosine triphosphate mediated steps to capture misfolded proteins, free them from local energy minima and finally provide them with an environment conducive to folding to their native states [20 – 23].

Small cantilever [24] AFMs can be used for making faster and quieter measurements [25]. A prototype small cantilever atomic force microscope [26] was used to observe, in real time, the interactions between individual molecules of the chaperonin protein GroES binding to and then dissociating from individual GroEL proteins, which were immobilized on a mica support [27]

Both GroEL and the GroEL–GroES complex monolayer in buffer solution were repeatedly imaged without the aid of fixing agents (Figs. 15 and 16). The central channel of the protein ring can be resolved on many of the molecules, indicating that GroEL adsorbs to mica in an end-up orientation. The average diameter of the molecules in this image is 14.6 ± 2.2 nm, which agrees well with both X-ray [28] and cryoelectron microscopy [29] data.

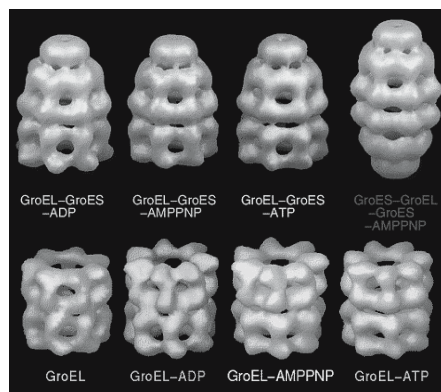


Figure 14. Cryo-electron microscopy images of the GroEL- and the GroEL-GroES-nucleotide structures at 30 Å resolution. Reprinted with permission from [30].

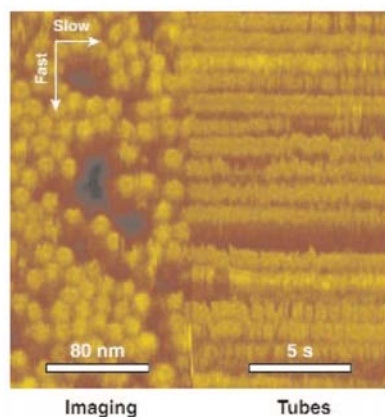


Figure 15. GroEL scanned in two dimensions (left) and in one dimension (right). In this image of GroEL, the slow scan axis was disabled half way through the scan. After the slow scan axis was disabled, the tip repeatedly scanned the same line of proteins, thereby generating protein ‘tubes’. Each tube corresponds to an individual protein molecule. Reprinted with permission from [27].

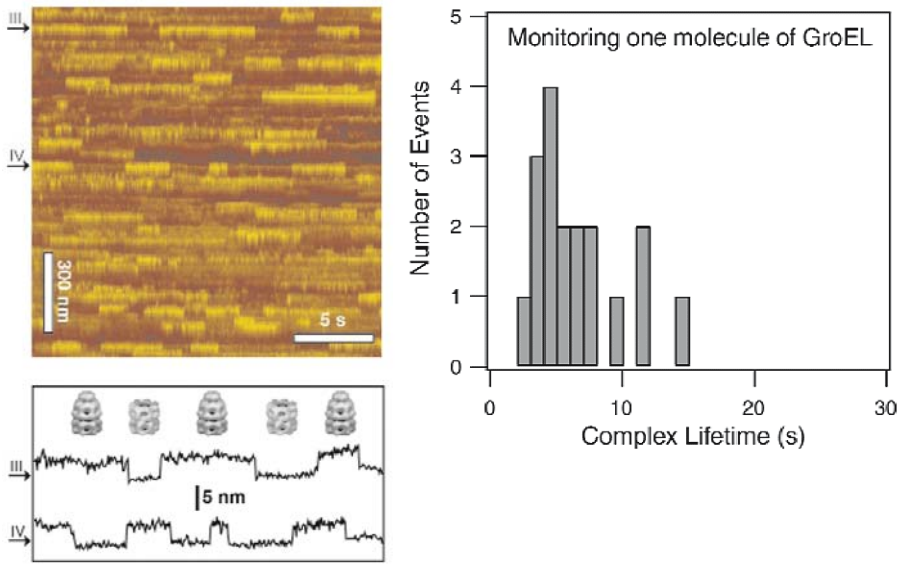


Figure 16. Left: After the addition of GroES and Mg-ATP into the buffer solution, large repeated variations in height along the lengths of many tubes are observed. Left bottom: The cross sections of these tubes show the height stepping between two values that differed by 3.6 ± 1 nm. Cryoelectron microscopy images by [30]. Right: Histogram of measured complex lifetime of an individual GroEL molecule in the presence of Mg-ATP and GroES. Individual GroES molecules attach to and then separate from the same GroEL molecule 18 times during an observation period of ~ 2 min. Note the absence of events with lifetimes < 2 s. Reprinted with permission from [27].

In order to obtain the temporal resolution required for observing the formation and dissociation of the GroEL–GroES complexes in the presence of Mg-ATP, we scanned the sample in one dimension rather than two. By repeatedly scanning a single line across the sample we were able to monitor the height of a series of protein molecules at rates as high as 20 Hz. This method is illustrated in Figure 16, which shows an image of GroEL molecules in buffer in which the slow scan axis was disabled half way through the scan. From this image it is clear that each ‘tube’ is associated with a single protein molecule. The height variations along the length of the tubes reflect the time dependent changes in the protein structure.

Upon the addition of both GroES and Mg-ATP, it was observed that many of the tubes displayed repeating well-defined step-like variations in height (Fig. 16, top left). The cross section of the two featured tubes clearly shows the step-like variations in height (Fig. 16, bottom left). The magnitude of these steps is 3.6 ± 1 nm. This is consistent with the height difference measured between structures of GroEL and the GroEL–GroES complex obtained by X-ray crystallography [28] and cryoelectron microscopy [29] studies. We therefore conclude that the observed height variations are caused

by a GroES molecule attaching to and then separating from the GroEL molecule associated with the tube.

In one case, we recorded an active molecule for ~ 2 min and saw the complex form and dissociate 18 times. A histogram of the complex lifetime for this molecule is shown in Figure 16, right. The distribution of complex lifetime has a maximum near 5 s and the average lifetime is $\sim 7 \pm 1$ s ($n = 18$).

4. NANOSTRUCTURING ATOMICALLY FLAT SURFACES WITH IONS

Most of the small structures currently used in technology are in the micrometer range. One reason for this is silicon micromachining technology, which works fast and at low cost in this regime. However, needs for increased data-storage density and smaller devices call for nanometer-sized structures.

In the following, a gentle technique to nanostructure surfaces is demonstrated: bombardment with so-called “slow” multicharged ions.

The AFM is the microscope of choice for investigating ion induced nanodefects on flat crystals, because of its great resolution and of the fact that it can image insulating materials.

One important way to produce nanostructures on surfaces involves kinetic sputtering by “fast” ions. However, fast ions unavoidably cause unwanted radiation damage. As opposed to this, potential sputtering (PS), i.e. desorption induced by the potential energy of slow multiply charged ions (MCI), holds great promise for more gentle nanostructuring [31, 32]. It can cause high sputter yields even at such low ion impact energies where kinetic sputtering and defect creation in deeper layers is not possible. While the physical mechanisms of PS have been the subject of extensive investigation [33 – 37], technical applications of slow MCI have so far remained largely unexplored, despite the fact that they provide unique opportunities for etching, ultra-thin film growth and nanostructure fabrication.

4.1. STM and AFM Investigations of HOPG Bombarded with Argon Ions

Highly oriented pyrolytic graphite (HOPG) is a crystalline layered material, that can easily be cleaved with an adhesive tape to obtain atomically flat surfaces (for STM and AFM images in atomic resolution, imaged in ultra high vacuum (UHV), see Fig. 17).

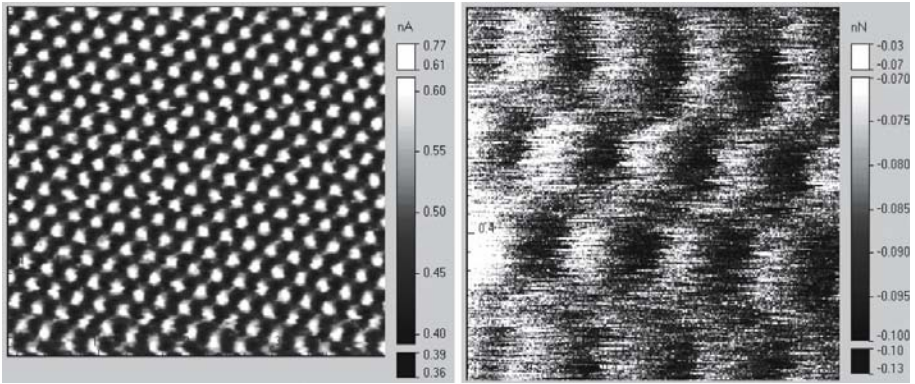


Figure 17. Highly oriented pyrolytic graphite imaged in ultrahigh vacuum with atomic resolution. Left: Scanning tunnelling microscopy image, image size $4 \times 4 \text{ nm}^2$. Right: Atomic force microscopy image, image size $1 \times 1 \text{ nm}^2$.

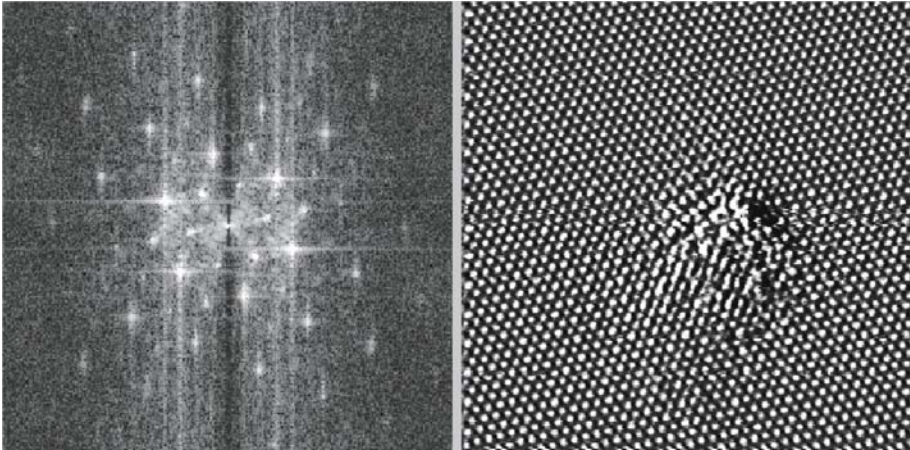


Figure 18. Highly oriented pyrolytic graphite bombarded with 800 eV Ar^+ ions imaged in ultrahigh vacuum with atomic resolution (right). The fourier transform (left) of the Ar^+ ion-induced defect reveals a $\sqrt{3} \times \sqrt{3}R30$ surface.

Bombardment with 800 eV Ar^+ ions and subsequent imaging with UHV STM reveals a $\sqrt{3} \times \sqrt{3}R30$ surface, as is characteristic for interstitial defects or vacancies in HOPG, surrounded by undisturbed surface regions (Figure 18).

Scanning with the AFM at atomic resolution on the irradiated surface did not show any significant topological changes due to ion bombardment. Therefore, it was concluded that the defects observed are mainly due to changes in the electronic density of states of the surface.

For more detailed information on these studies, see [38, 39].

4.2. Ion Bombardement of Atomically Flat Insulator Crystals

We carried out a systematic search for PS with atomically clean monocrystalline insulator targets which have been bombarded by low-energy ions on the single impact level, searching for resulting surface defects by means of AFM.

The targets remained under UHV conditions during ion irradiation and subsequent AFM inspection.

The insulators studied included LiF(100), SiO₂(0001) α -quartz, muscovite mica and sapphire c-plane Al₂O₃(0001) after their irradiation with low doses of slow singly- and multiply-charged ions.

Ion bombardment was performed at a dose of $5 \cdot 10^{12}$ ions/cm², which is equivalent to five incident ions per $10 \cdot 10$ nm square. Ion bombardment was accompanied by low-energy electron flooding to compensate for surface charging which otherwise would have strongly inhibited the AFM observation.

Resulting nanostructures on the surfaces as investigated by AFM are hillocks a few nanometers high.

Of all crystals investigated, Al₂O₃ showed the most promising results (the size of the hillocks increased with increasing potential energy of the ions with which the samples were bombarded, see Figure 19). For SiO₂ further research might lead to a similar conclusion.

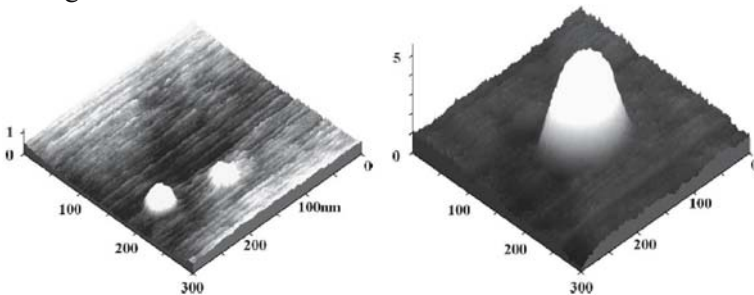


Figure 19. UHV AFM contact mode image of sapphire (Al₂O₃, c-plane 0001) bombarded with 500 eV Ar⁺ (left image) and Ar⁷⁺ (right image) ions. The nanodefects induced by Ar⁷⁺ ions (same kinetic but higher potential energy than the Ar⁺ ions) are considerably higher and wider than those caused by singly charged ions. The defects are real topographic features; all dimensions in nanometers. Reprinted with permission from [39].

Both materials are of great relevance for applications in a rapidly emerging field combining microelectronics and nanotechnology.

For detailed descriptions of these studies, see [39, 40].

4.3. Surface Modifications on Si(111) Produced by the Impact of Slow Multiply Charged Ions

We are currently investigating whether beams of slow MCI can be utilized to produce nanometer-sized surface modifications on silicon substrates. In particular, hydrogen-terminated Si(111) surfaces shall be bombarded in UHV with low fluxes of slow MCI.

Due to MCI - surface interaction the hydrogen atoms should be removed around the MCI impact site and the resultant dangling silicon bonds should then react with oxygen introduced into the UHV chamber so producing ultra-shallow silicon oxide nanodots.

The formation of such nanostructures at ion impact sites is going to be studied with AFM and STM in UHV.

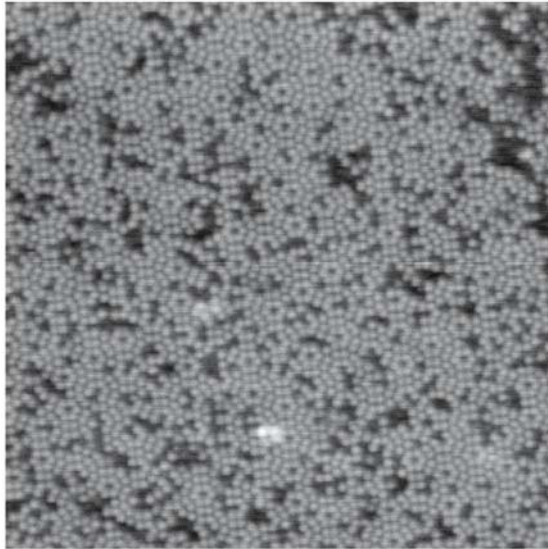


Figure 20. STM image (topography, raw data) of the reconstructed Silicon (111)-(7*7) surface. Scan size 40*40 nm², sample bias +1 V (empty-states tunnelling), tunnelling current 1.2 nA, scanning speed 80 nm/s.

Figure 20 shows an UHV STM image of the sample we are going to use for these studies, namely the reconstructed Silicon(111)(7*7) surface. This sample was prepared in a UHV chamber with a pressure of approximately 2.5×10^{-10} mbar. Several steps of heating were used to induce desorption of gases. The first step was radiative heating for 3 hours to remove adsorbed gas from the surrounding components. The subsequent outgassing steps were achieved by passing a current through the sample; the sample details are boron-doped silicon, 0.01-0.02 ohm cm, 13*3*0.5 mm³ dimensions. The first step was carried out with a current of approximately 1.4 A through the

sample; at this point the sample was just below the temperature where glowing becomes visible (approximately 500-600 C). After this step, a series of short heating pulses with increasing current and therefore sample temperature followed, beginning with 5 A, then 6 A and then up to 10 A. These steps were accompanied by pulses of pressure that died away after ~1 minute. The last 10 A step corresponded to a temperature of approximately 1280° C as measured by a pyrometer. After about 10 seconds the current was reduced first to one half and then it was reduced by 0.1 A per 5 seconds. The sample was allowed to cool for about 1 hour before transfer to the AFM/STM unit for studying.

5. SUBATOMIC FEATURES

5.1. Atomic Orbitals in Tungsten

In July 2004, a breakthrough in the resolving power of microscopy was reported by a team of physicists at Augsburg University [41]. An individual tungsten atom was imaged by atomic force microscopy at a resolution of 77 pm. The diameter of a carbon atom is 142 picometers, the diameter of a tungsten atom is 274 picometers. Four distinct peaks that are attributed to highly localized electron clouds can be identified (see Figure 21).

The experiment was performed in UHV at five degrees Kelvin. The microscope was isolated from vibrations by a 30 t foundation and from sound and electromagnetic stray fields by a metal chamber.

Whereas STM only probes the most loosely bound electrons with an energy at the Fermi level, AFM can resolve the charge density variations within a single atom, because the forces between the AFM tip and the sample are of electrostatic nature.

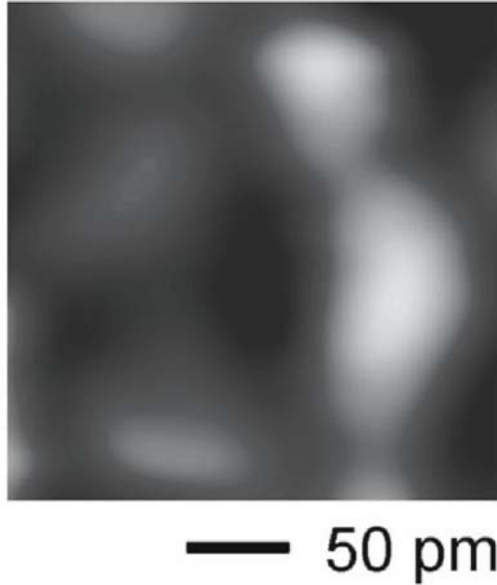


Figure 21. UHV low temperature (5 K) AFM constant-height mode image reveals four-fold symmetry in the amplitudes of the higher harmonics V_{hh} signal (centered close to the maximum of the tunnelling current, data not shown). The symmetry of the V_{hh} signals points to the fourfold bonding symmetry of the W atom viewed parallel to a $\langle 001 \rangle$ crystal direction. Reprinted with permission from [41].

The electron structure originates from the quantum-mechanical nature of tungsten bonding. Tungsten develops a body centred cubic crystal structure such that every tungsten atom is surrounded by eight nearest neighbour atoms, causing "arms" of increased charge density which point to the next neighbours. Four of these highly localized electron clouds are visible on surface atoms.

The role of tip and sample was switched in the experiment: the front atom in a sharp tungsten tip was imaged by a light carbon atom of a graphite surface. The reason a light atom was used for probing was to minimize image blurring, since the mapping of one atom with another atom always involves a convolution of the electronic states. The tunnelling current is confined to the top atom because of the sharp increase of tunnelling probability with decreasing distance.

Instead of measuring static deflections or frequency changes, higher harmonics triggered by tip-sample forces (V_{hh}) are analyzed in this technique. The higher harmonics are much more sensitive to short-range interactions than the previously used signals.

5.2. Electron Spins

In 1990 John Sidles set himself the problem of locating the atoms in a single protein molecule. His idea to combine magnetic resonance (MR) with force microscopy in magnetic resonance force microscopy (MRFM) was published as a concept in 1991 [42].

Sidles settled on force microscopy because the performance of induction coils, the detectors in conventional MR, scales unfavourably with size. At least 10^{12} nuclear spins are needed to yield a detectable signal. Shrinking the coil to encompass fewer spins reduces the signal irretrievably below noise. A force microscope, on the other hand, becomes more sensitive the smaller it gets.

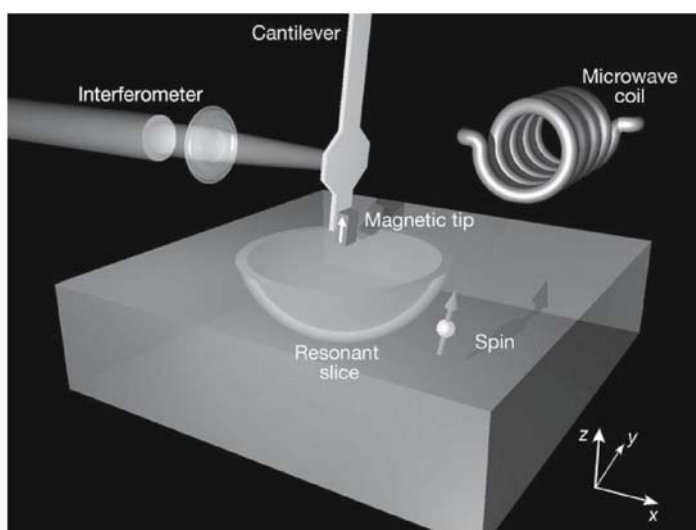


Figure. 22. Configuration of the single-spin MRFM experiment. The magnetic tip at the end of an ultrasensitive silicon cantilever is positioned approximately 125 nm above a polished SiO_2 sample containing a low density of unpaired electron spins. Spins as deep as 100 nm below the sample surface can be probed. Reprinted with permission from [43].

In 2004, Rugar and co-workers improved MRI sensitivity by some 10 million times compared with the medical MRI devices used to visualize organs in the human body. The improved sensitivity extends MRI into the nanometer realm and now allows for single electron spin detection [43].

In their MRFM, a small strong ferromagnetic CoSm dot is mounted on the sharp cantilever, yielding a field gradient of 2 G/nm. Experiments are performed at a temperature of 1.6 K.

The test sample was vitreous silica, which had been bombarded with a 2-Gy dose of Co^{60} γ -rays, yielding 10^{13} to 10^{14} unpaired electron spins (E' centers) per cubic centimeter.

Unpaired electrons and many atomic nuclei behave like tiny bar magnets. The force exerted by an electron spin on the cantilever is a few attonewtons (10^{-18} N). Such a force is roughly 10 million million times smaller than the force a snowflake exerts resting on your hand. Such a force is even a million times weaker than the forces usually encountered in atomic force microscopy.

Detecting such a small force requires a pliable cantilever. Yet, a pliable cantilever, unlike stiffer AFM cantilevers, can't be positioned close to a surface because the tip would stick to it. Therefore, the cantilever in MRFM is held perpendicular to the sample surface and deflects when a spin lies in front or behind rather than directly below (Fig. 22). A laser interferometer records the cantilever deflections and sophisticated measurement signal acquisition techniques and long measurement times are needed for successful single spin detection.

Several other single-spin detection methods have previously been demonstrated [44 – 50]; see Figure 23 for an STM based method). Yet, MRFM has some attributes that set it apart: The MRFM can sense an electron lying dozens of atomic layers beneath the surface. It is a major milestone toward creating a microscope that can make three-dimensional images of molecules with atomic resolution.

If developed further, the MRFM technique could prove useful for investigating the atomic structure inside materials used in the electronics industry and to image biomolecules – such as proteins - at atomic resolution. However, to reach this goal, nuclear spins have to be detected. Nuclear spins are harder to detect than electron spins, because a proton's magnetic moment is 658 times weaker than that of an electron.

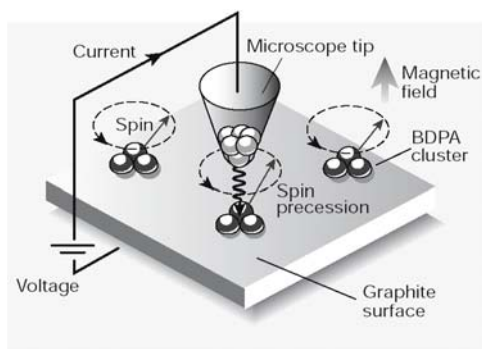


Figure. 23. Spin detection through the union of high-resolution microscopy and resonance techniques. A graphite surface is coated with clusters of organic BDPA molecules. In the applied magnetic field, the electron-spin vectors (red arrows) associated with free radicals in the molecules precess at a certain frequency. When the tip of a scanning tunneling microscope is brought close to a cluster, the tunnelling current is modulated at the precession frequency; detecting the modulation effectively measures electronic spin in the molecule. Reprinted with permission from [51].

6. CONCLUSIONS AND OUTLOOK

In this review, we presented scanning probe microscopy across dimensions, from large samples like single cells, to single biomolecules and nanometer small ion induced defects on crystal surfaces to subatomic features like orbitals and single spins.

Scanning probe microscopy has even left the surface regime. MFRM promises to be one of the most powerful tools to reach our goal: the 3D-imaging of molecules, at surfaces or in bulk state, at atomic resolution.

7. ACKNOWLEDGEMENTS

Part of this work has been supported by the Austrian FWF (Project No. P-16178) and was carried out at Vienna University of Technology.

Part of this work was funded from the "Austrian Kplus-Program" and has been carried out at the "Austrian Center of Competence for Tribology", AC²T research GmbH.

8. REFERENCES

1. Binnig G., Rohrer H., Gerber Ch. and Weibel E. Surface studies by scanning tunneling microscopy. *Phys. Rev. Lett.* 1982; 49: 57-61.
2. Binnig G., Quate C.F., and Gerber Ch. Atomic force microscope, *Phys. Rev. Lett.* 1986; 56: 930-933.
3. Pohl D.W., Denk W., and Lanz M. Optical stethoscopy: Image recording with resolution $\lambda/20$, *Appl. Phys. Lett.* 1984; 44(7): 651-653.
4. Morris V.J., Kirby A.R. and Gunning A.P. *Atomic Force Microscopy for Biologists*. World Scientific Publishing Company, 1999
5. Hartmann U. An elementary introduction to atomic force microscopy and related methods, PDF document from the Institute of Experimental Physics, Univ. of Saarbrücken (www.uni-saarland.de/fak7/hartmann/download/afm/afm.pdf)
6. Binnig G. and Rohrer H. The Scanning Tunneling Microscope. *Scientific American* 1985; 253: 50-56.
7. Quate C.F. Vacuum Tunneling: A New Technique for Microscopy. *Physics Today* 1986; 39: 26-33.
8. Binnig G. and H. Rohrer In touch with atoms. *Rev. Mod. Phys.* 1999; 71(2): S324-S330.
9. Hansma P.K., Cleveland J.P., Radmacher M., Walters D.A., Hillner P.E., Bezanilla M., Fritz M., Vie D., Hansma H.G., Prater C.B., Massie J., Fukunaga L., Gurley J. and Elings V. Tapping mode atomic force microscopy in liquids. *Appl. Phys. Lett.* 1994; 64(13): 1738-1740.
10. Prater C.B., Hansma P.K., Tortonese M. and Quate C.F. Improved scanning ion-conductance microscope using microfabricated probes. *Rev. Sci. Instrum.* 1991; 62(11): 2635-2638.
11. Hansma P.K., Drake B., Marti O., Gould S.A. and Prater C.B. The scanning ion-conductance microscope. *Science* 1989; 243(4891): 641-643.
12. Schraml S. Setup and application of a Scanning Ion Conductance Microscope, Diploma thesis, Vienna University of Technology, Austria, 2003

13. Werner D. *The biology of diatoms*. University of California Press, 1977
14. Round F.E., Crawford R.M. and Mann D.G. *Diatoms: Biology and morphology of the genera*. Cambridge University Press., 1990
15. Gebeshuber I.C., Thompson J.B., Del Amo Y., Stachelberger H. and Kindt J.H. In vivo nanoscale atomic force microscopy investigation of diatom adhesion properties. *Materials Science and Technology* 2002; 18: 763-766.
16. Gebeshuber I.C., Kindt J.H., Thompson J.B., Del Amo Y., Stachelberger H., Brzezinski M., Stucky, G.D. Morse D.E. and Hansma P.K. Atomic force microscopy study of living diatoms in ambient conditions. *J. Microsc.* 2003; 212: 292-299.
17. Smith B.L., Schäffer T.E., Viani M., Thompson J.B., Frederick N.A., Kindt J., Belcher A., Stucky G.D., Morse D.E. and Hansma P.K. Molecular mechanistic origin of the toughness of natural adhesives, fibres and composites. *Nature* 1999; 399: 761-763.
18. Gebeshuber I.C., Stachelberger H. and Drack M. Diatom bionanotribology - Biological surfaces in relative motion: their design, friction, adhesion, lubrication and wear. *J. Nanosci. Nanotechnol.* 2005; 5: 1-9.
19. Gebeshuber I.C., Stachelberger H. and Drack M. "Surfaces in relative motion: bionanotribological investigations." In: *First International Industrial Conference Bionik 2004*, I. Boblan and R. Bannasch, eds. Düsseldorf: VDI Verlag 2004. ISBN 3-18-324915-4, ISSN 0178-9589229-236, 229-236, 2004.
20. Hartl F.U. Molecular chaperones in cellular protein folding. *Nature* 1996; 381: 571-580.
21. Ranson N.A., White H.E. and Saibil H.R. Chaperonins. *Biochem J.* 1998; 333(2): 233-242.
22. Sigler P.B., Xu Z., Rye H.S., Burston S.G., Fenton W.A. and Horwich A.L. Structure and function in GroEl-Mediated protein folding. *Annu. Rev. Biochem.* 1998; 67: 581-608.
23. Fink A.L. Chaperone-Mediated Protein Folding. *Physiol. Rev* 1999; 79(2): 425 - 449.
24. Walters D.A., Cleveland J.P., Thomson N.H., Hansma P.K., Wendman M.A., Gurley G. and Elings V. Short cantilevers for atomic force microscopy. *Rev. Sci. Instrum.* 1996; 67(10): 3583-3590.
25. Viani M.B., Schäffer T.E., Chand A., Rief M., Gaub H.E. and Hansma P.K. Small cantilevers for force spectroscopy of single molecules. *J. Appl. Phys.* 1999; 86(4): 2258–2262.
26. Viani M.B., Schäffer T.E., Palocz G.T., Pietrasanta L.I., Smith B.L., Thompson J.B., Richter M., Rief M., Gaub H.E., Plaxco K.W., Cleland A.N., Hansma H.G. and Hansma P.K. Fast imaging and fast force spectroscopy of single biopolymers with a new atomic force microscope designed for small cantilevers. *Rev. Sci. Instrum.* 1999; 70(11): 4300–4303.
27. Viani M.B., Pietrasanta L.I., Thompson J.B., Chand A., Gebeshuber I.C., Kindt J.H., Richter M., Hansma H.G. and Hansma P.K. Probing protein-protein interactions in real time. *Nature Structural Biology* 2000; 7: 644-647.
28. Braig K., Otwinowski Z., Hegde R., Boisvert D.C., Joachimiak A., Horwich A.L. and Sigler P.B. The crystal structure of the bacterial chaperonin GroEL at 2.8 Å. *Nature* 1994; 371: 557-559.
29. Xu Z., Horwich A.L. and Sigler P.B. The crystal structure of the asymmetric GroEL-GroES-(ADP)₇ chaperonin complex. *Nature* 1997; 388: 741-750.
30. Roseman A.M., Chen S., White H., Braig K. and Saibil H.R. The chaperonin ATPase cycle: mechanism of allosteric switching and movements of substrate-binding domains in GroEL. *Cell* 1996; 87: 241–251.
31. Winter HP. and Aumayr F. Slow multicharged ions hitting a solid surface: From hollow atoms to novel applications. *Europhys. News* 2002; 6: 215-217.
32. Arnau A., Aumayr F., Echenique P.M., Grether M., Heiland W., Limburg J., Morgenstern R., Roncin P., Schippers S., Schuch R., Stolterfoht N., Varga P., Zouros T.J.M. and Winter HP. Interaction of slow multicharged ions with solid surfaces. *Surf. Sci. Rep.* 1997; 27: 113 – 240.

33. Sporn M., Libiseller G., Neidhart T., Schmid M., Aumayr F., Winter HP., Varga P., Grether M., Niemann D. and Stolterfoht N. Potential sputtering of clean SiO₂ by slow highly charged ions. *Phys. Rev. Lett.* 1997; 79: 945–948.
34. Aumayr F., Burgdörfer J., Varga P. and Winter HP. Sputtering of insulator surfaces by slow highly charged ions: "coulomb explosion" or "defect-mediated desorption"? *Comm. Atom. Molecul. Phys.* 1999; 34: 201-219.
35. Schenkel T., Hamza A.V., Barnes A.V. and D.H. Schneider Interaction of slow, very highly charged ions with surfaces. *Progr. Surf. Sci.* 1999; 61: 23-84.
36. Hayderer G., Cernusca S., Schmid M., Varga P., Winter HP., Aumayr F., D. Niemann, Hoffmann V., Stolterfoht N., Lemell C., Wirtz L. and Burgdörfer J. Kinetically-assisted potential sputtering of insulators by highly charged ions. *Phys. Rev. Lett.* 2001; 86: 3530-3533.
37. Hayderer G., Schmid M., Varga P., Winter HP., Aumayr F., Wirtz L., Lemell C., Burgdörfer J., Hägg L. and Reinhold C.O. Threshold for potential sputtering of LiF. *Phys. Rev. Lett.* 1999; 83: 3948-3951.
38. Hayderer G., Cernusca S., Schmid M., Varga P., Winter HP. and Aumayr F. STM studies of HCl-induced surface damage on highly oriented pyrolytic graphite. *Physica Scripta* 2001; T92: 156-157.
39. Gebeshuber I.C., Cernusca S., Aumayr F. and Winter HP. Nanoscopic surface modification by slow ion bombardment. *Int. J. Mass Spectrometry* 2003; 229(1-2): 27-34.
40. Gebeshuber I.C., Cernusca S., Aumayr F. and Winter HP. Slow multicharged-ion induced nanodefects on monocrystalline insulator surfaces studied by UHV-AFM. *Nucl. Instr. Meth. Phys. Res. B* 2003; 205: 751-757.
41. Hembacher S., Giessibl F.J., Mannhart J. Force microscopy with light atom probes. *Science* 2004; 305: 380-383.
42. Sidles J.A. Noninductive detection of single-proton magnetic resonance. *Appl. Phys. Lett.* 1991; 58: 2854-2856.
43. Rugar D., Budakian R., Mamin H.J. and Chui B.W. Single spin detection by magnetic resonance force microscopy. *Nature* 2004; 430: 329-332.
44. Manassen Y., Hamers R.J., Demuth J.E. and Castellano A.J. Direct observation of the precession of individual paramagnetic spins on oxidized silicon surfaces. *Phys. Rev. Lett.* 1989; 62: 2531–2534.
45. Durkan C. and Welland M.E. Electronic spin detection in molecules using scanning-tunnelingmicroscopy-assisted electron-spin resonance. *Appl. Phys. Lett.* 2002; 80: 458–460.
46. Wrachtrup J., von Borzyskowski C., Bernard J., Orritt M. and Brown R. Optical-detection of magnetic resonance in a single molecule. *Nature* 1993; 363: 244–245.
47. Köhler J., Disselhorst J.A.J.M., Donckers M.C.J.M., Groenen E.J.J., Schmidt J. and Moerner W.E. Magnetic resonance of a single molecular spin. *Nature* 1993; 363: 242–244.
48. Jelezko F., Popa I., Gruber A., Tietz C., Wrachtrup J., Nizovtsev A. and Kilin S. Single spin states in a defect center resolved by optical spectroscopy. *Appl. Phys. Lett.* 2002; 81: 2160–2162.
49. Elzerman J.M., Hanson R., Willems van Beveren L.H., Witkamp B., Vandersypen L.M.K. and Kouwenhoven L.P. Single-shot read-out of an individual electron spin in a quantum dot. *Nature* 2004; 430: 431-435.
50. Xiao M., Martin I., Yablonovitch E. and Jiang H.W. Electrical detection of the spin resonance of a single electron in a silicon field-effect transistor. *Nature* 2004; 430: 435-439.
51. Manoharan H.C. Applied physics: Spin spotting. *Nature* 2002; 416: 24-25.